Structures and non-linear optical properties of polar carotenoid analogues*

Hideki Hashimoto,[1,†] Takayasu Nakashima,[1] Kingo Hattori,[1] Takashi Yamada,[1] Tadashi Mizoguchi,[2] Yasushi Koyama[2] and Takayoshi Kobayashi[3]

[1]*Department of Materials Science and Chemical Engineering, Faculty of Engineering, Shizuoka University, 5-1 Johoku 3-Chome, Hamamatsu 432-8561, Japan*
[2]*Faculty of Science, Kwansei Gakuin University, 1-1-155 Uegahara, Nishinomiya 662-8501, Japan*
[3]*Department of Physics, Graduate School of Science, University of Tokyo, Hongo 7-3-1, Bunkyo-ku, Tokyo 113-0033, Japan*

Abstract: The structures and non-linear optical properties of polar carotenoid analogues, in which electron-accepting groups were introduced to the polyene backbone of carotenoids, were studied. Molecular and crystal structures of a novel polar carotenoid analogue β-ionylidene-2,4-dinitrophenylhydrazone, that is applicable as a second-order non-linear optical material, are introduced. Stark spectroscopy, in order to determine the non-linear polarizabilities, is demonstrated. Non-linear polarizabilities of indan-1,3-dione and its mono- and bis-dicyanomethylene derivatives of retinal, that are applicable as third-order non-linear optical materials, are introduced.

INTRODUCTION

Molecules with large optical non-linearities are required for photonic applications, including all-optical switching and data processing [1–5]. Table 1 summarizes various non-linear optical effects. The non-linear optical processes are governed by non-linear susceptibilities (χ) of materials. Depending on the number of applied electric fields, the non-linear susceptibilities are classified into second order, third order, and so on. In the case of conventional laser intensity, the non-linear polarization and hence the size of the non-linear effect decrease with an increase in the order of the susceptibility. Therefore, the non-linearity up to the third order is used in practical applications. The non-linear optical effects can be classified into two categories: one concerned with frequency conversion and marked with filled circles (●), and the other concerned with optical modulation and marked with open circles (○). Although it is well known that many organic materials possess a much larger non-linearity than that of inorganic materials, owing to their poor durability and also due to the intervention of blue–green diode lasers, the application of organic materials to frequency conversion is no longer promising. On the other hand, the application of organic materials to optical modulation has attracted much attention recently.

The non-linearity of organic materials, except conjugated polymers and coherent aggregates of dye molecules, depends solely on the non-linear polarizability of the component molecule. A molecular polarizability can be expanded in terms of a power series of applied electric fields, and is expressed as shown in Eqn (1) [2].

$$p_i^\omega = p_i^{0,\omega} + \alpha_{ij}E_j^\omega + \beta_{ijk}E_j^{\omega 1}E_k^{\omega 2} + \gamma_{ijkl}E_j^{\omega 1}E_k^{\omega 2}E_l^{\omega 3} \tag{1}$$

Table 1 Passive/active, linear/non-linear optical processes

Angular frequency of incident wave	Angular frequency of generated electric polarization	Electric susceptibility	Optical process
(1) Passive linear optical effect			
ω	No polarization	0	Propagation in vacuum
ω	ω	$\chi^{(1)}(-\omega; \omega)$	Linear scattering
(2) Passive non-linear effect			
(2.1) Second order			
ω_1, ω_2	$\omega_3 \ (= \omega_1 + \omega_2)$	$\chi^{(2)}(-\omega_3; \omega_1, \omega_2)$	Sum-frequency generation (●)
ω	2ω	$\chi^{(2)}(-2\omega; \omega, \omega)$	SHG (●)
$\omega, 0$	ω	$\chi^{(2)}(-\omega; \omega, 0)$	Linear electro-optic effect (Pockels effect) (○)
ω_1	ω_2, ω_3 (where $\omega_2 + \omega_3 = \omega_1$)	$\chi^{(2)}(-\omega_3; \omega_1, \omega_2)$	Three-wave parametric fluorescence (●)
ω_1, ω_2	ω_3 (where $\omega_3 = \omega_1 - \omega_2$)	$\chi^{(2)}(-\omega_3 : -\omega_2, \omega_1)$	Three-wave difference-frequency generation (three-wave parametric mixing (amplification, oscillation)) (●)
2ω	ω	$\chi^{(2)}(-\omega; -\omega, 2\omega)$	Degenerate three-wave difference-frequency generation (●)
ω	0	$\chi^{(2)}(0; -\omega, \omega)$	Inverse linear EO effect (optical rectification) (○)
(2.2) Third order			
$\omega_1, \omega_2, \omega_3$	$\omega_4 \ (= \omega_1 + \omega_2 + \omega_3)$	$\chi^{(3)}(-\omega_4; \omega_1, \omega_2, \omega_3)$	Four-wave sum-frequency mixing (●)
ω	3ω	$\chi^{(3)}(-3\omega; \omega, \omega, \omega)$	THG (●)
ω_1, ω_2	ω_3, ω_4 (where $\omega_1 + \omega_2 = \omega_3 + \omega_4$)	$\chi^{(3)}(-\omega_3; \omega_4, \omega_1, \omega_2)$ $\chi^{(3)}(-\omega_4; \omega_3, \omega_2)$	Four-wave difference-frequency mixing (four-wave parametric mixing (amplification, oscillation)) (●)
ω	ω	$\chi^{(3)}(-\omega; -\omega, \omega, \omega)$	Degenerate four-wave mixing (DFWM), optically induced change in refractive index, optical (ac, dynamic) Kerr effect, self-focusing, self-divergence, self-phase modulation (○)
$\omega, 0$	ω	$\chi^{(3)}(-\omega; 0, 0, \omega)$	Non-linear (secondary) EO effect ((dc) Kerr effect) (○)
$\omega, 0$	2ω	$\chi^{(3)}(-2\omega; 0, \omega, \omega)$	Direct current electric field-induced SHG (DCSHG or EFISH) (●)
(3) Active linear optical effect			
ω	ω	$\chi^{(1)}(-\omega; \omega)$	Linear absorption/amplification ($\omega \approx \omega_{10}$ transition energy)
(4) Active non-linear optical effect			
(4.1) Third order			
ω_1	ω_2	$\chi^{(3)}(-\omega_2; \omega_1, -\omega_1, \omega_2)$	Raman scattering ($|\omega_1 - \omega_2| = \omega_{10}$; optical phonon) Brillouin scattering ($|\omega_1 - \omega_2| = \omega_{10}$; acoustic phonon)
ω	ω	$\chi^{(3)}(-\omega; \omega, -\omega, \omega)$	Degenerate two-photon absorption ($2\omega \approx \omega_{10}$)
ω_1, ω_2	ω_1, ω_2	$\chi^{(3)}(-\omega_2; \omega_1, -\omega_1, \omega_2)$ $\chi^{(3)}(-\omega_1; \omega_2, -\omega_2, \omega_1)$	Non-generate two-photon absorption ($\omega_1 + \omega_2 \approx \omega_{10}$) ($\omega_1 + \omega_2 = \omega_{10}$)
ω	ω	$\chi^{(3)}(-\omega; \omega, -\omega, \omega)$	Absorption saturation
(4.2) Fifth order			
ω_1	ω_2	$\chi^{(5)}(-\omega_2; \omega_1, -\omega_1, \omega_1, -\omega_1, \omega_2)$	Hyper-Raman scattering

EO, electro-optic; SHG, second harmonic generation; THG, third harmonic generation.

Here, α is a linear polarizability, and β and γ are the first- and second-order hyperpolarizabilities, respectively. The magnitude of these non-linear polarizabilities has a close relation with the molecular structure. Macroscopic polarizabilities of crystals are defined as susceptibilities (χ), and are expressed as shown in Eqn (2) [2].

$$\chi_{IJ}^{(1)} = NF_I^{\omega_I}F_J^{\omega_J} \sum_{s=1}^{n} \cos[I,i(s)] \cos[J,j(s)]\alpha_{ij}(s) \tag{2a}$$

$$\chi_{IJK}^{(2)} = NF_I^{\omega_I}F_J^{\omega_J}F_K^{\omega_K} \sum_{\substack{s=1 \\ i,j,k}}^{n} \cos[I,i(s)] \cos[J,j(s)] \cos[K,k(s)]\beta_{ijk}(s) \tag{2b}$$

$$\chi_{IJKL}^{(3)} = NF_I^{\omega_I}F_J^{\omega_J}F_K^{\omega_K}F_L^{\omega_L} \sum_{\substack{s=1 \\ i,j,k,l}}^{n} \cos[I,i(s)] \cos[J,j(s)] \cos[K,k(s)] \cos[L,l(s)]\gamma_{ijkl}(s) \tag{2c}$$

Here, I, J and K denote the crystal axes, and i, j and k denote the molecular axes. F is the local field correction factor, and N represents the number density of molecules. In the case of a weak interaction limit, the macroscopic susceptibilities can be expressed as a vector summation of microscopic molecular polarizabilities. Therefore, the magnitude of susceptibilities is highly dependent on the molecular arrangement in a crystal.

In order to optimize the performance of the non-linear optical materials, it is important to reveal the relation between structures and the non-linearity of molecules and crystals. We have taken both experimental and theoretical approaches to this problem, and have tried to develop a new class of non-linear organic materials using carotenoids as a structural motif.

STRUCTURES AND OPTICAL PROPERTIES OF β-IONYLIDENE-2,4-DINITROPHENYLHYDRAZONE

In this section, aimed at the development of better quality second-order non-linear materials, structures and optical properties of a novel polar carotenoid analogue, β-ionylidene-2,4-dinitrophenylhydrazone (β-IDNPH), are discussed.

The second-order non-linearity of materials can be used for the application of electro-optic sampling [6] and the production of terahertz (THz) radiation [7], i.e. coherent radiation in the far-infrared spectral region. In order for the materials to have a second-order non-linear activity, they must lack a centre of symmetry to avoid an offset effect. This is a fairly difficult condition to design into such materials, especially in a crystalline phase, because in such a case the materials must have spontaneous polarization, which can easily disappear due to repulsive electrostatic interaction between two neighbouring dipoles in a parallel configuration. However, some organic materials can satisfy this strict condition. We have already succeeded in developing organic crystals using derivatives of 4-nitro anilines and 4-cyano anilines, which have a large second-order susceptibility and a large enough size, together with excellent optical quality [8,9]. The hottest topic in this field is that we have recently succeeded in emitting THz radiation from these crystals with a comparable intensity to that of ZnTe, a well-known inorganic THz emitter [10,11]. With regard to the development of second-order non-linear materials, push–pull charge transfer hydrazones have attracted attention recently, because these materials produce single crystals that lack a centre of symmetry with more than 70% probability [12,13]. Based on this background, we have started to develop novel push–pull hydrazones using carotenoids as starting materials.

Molecular structure of β-IDNPH

Figure 1 shows the chemical structure of β-IDNPH. β-Ionone and 2,4-dinitrophenylhydrazine (DNPH) were coupled in the presence of a catalytic amount of *p*-toluene sulfonic acid, and β-IDNPH was obtained with a yield of 90.6%. All the ^{1}H and ^{13}C signals of β-IDNPH were assigned on the basis of ^{1}H–^{1}H NOESY, ^{1}H–^{1}H COSY, ^{13}C–^{1}H COSY, ^{13}C–^{1}H COLOC and ^{1}H–^{13}C HMBC two-dimensional (2D) nuclear magnetic resonance (NMR) measurements. Correlation found in 2D NMR spectra confirmed the

6s-*cis* configuration of the β-ionone ring, an anti structure of an N—N single bond, and the stereochemical structure around the N—C single bond as illustrated in Fig. 1. Judging from the 90% yield of the synthesis, this type of stereostructure can be produced selectively. Comparison of the corresponding chemical shifts of ^{1}H and ^{13}C signals among β-IDNPH, β-ionone and DNPH showed that the deviation of the chemical shifts is localized near the joint part of β-ionone and DNPH. This result suggests that β-IDNPH possesses a similar electronic structure to those of β-ionone and DNPH, except the joint part. This information is useful for the analysis of vibrational modes in β-IDNPH.
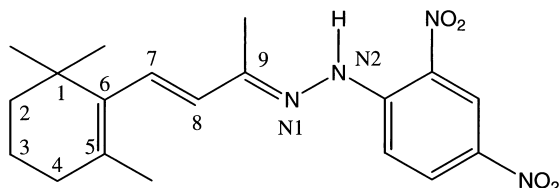
Fig. 1 Chemical structure of β-ionylidene-2,4-dinitrophenylhydrazone (β-IDNPH).

Crystal structure of β-IDNPH

Table 2 summarizes the results of X-ray crystallography. β-IDNPH shows a good crystal habit, and single crystals with a large enough size and enough optical quality can be produced without difficulty. However, it was very difficult to determine the crystal structure because of a large thermal deviation factor. In order to reduce this factor, we accumulated diffraction data at cryogenic temperature. Eventually, we determined the crystal structure at as low as −100 °C. However, *R*-values were still as high as 10%, and hence the molecular structures determined have some ambiguities.

Table 2 Crystal data of β-ionylidene-2,4-dinitrophenylhydrazone

Empirical formula	$C_{19}H_{24}N_4O_4$
Formula weight	372.42
Crystal colour, habit	Red, plate
Crystal system	Monoclinic
Lattice type	Primitive
Lattice parameters	$a = 8.597(4)$ Å
	$b = 34.103(4)$ Å
	$c = 13.170(3)$ Å
	$\beta = 96.85(3)°$
	$V = 3833(1)$ Å^3
Space group	$P2_1$(#4)
Z value	8
D_{calc}	1.290 g/cm^3
Residuals: *R*; *R*w	0.114; 0.138

The space group symmetry was determined to be $P2_1$, which lacks inversion symmetry, and hence the crystal has second-order non-linear activity. The *Z* value was determined to be 8, and hence four asymmetric molecules exist in each unit cell. The molecular structures (Types 1, 2, 3 and 4) of these asymmetric molecules are shown in Fig. 2. It is expected that these data will provide us with information concerning the intermolecular interaction in the crystals. For example, if we pay attention to the dihedral angle around the C6—C7 single bond, it was determined to be ± 50° or ± 40°. Molecular orbital calculations predict the stable structures at these particular angles. Therefore, this result suggests that the molecule in the crystal insists its integrity. Figure 3 compares the bond lengths of the four asymmetric molecules in the crystal. It is interesting to note that the Type 1 molecule shows strong polarization, while the Type 4 molecule shows good conjugation. The C9═N1 bond in the Type 1 molecule has a bond length

that is comparable with a triple bond, while that in Type 4 is between the lengths of a single and a double bond. As the Type 1 molecule is next to Type 4 in the crystal, the non-centrosymmetric crystal structure of β-IDNPH might be stabilized.
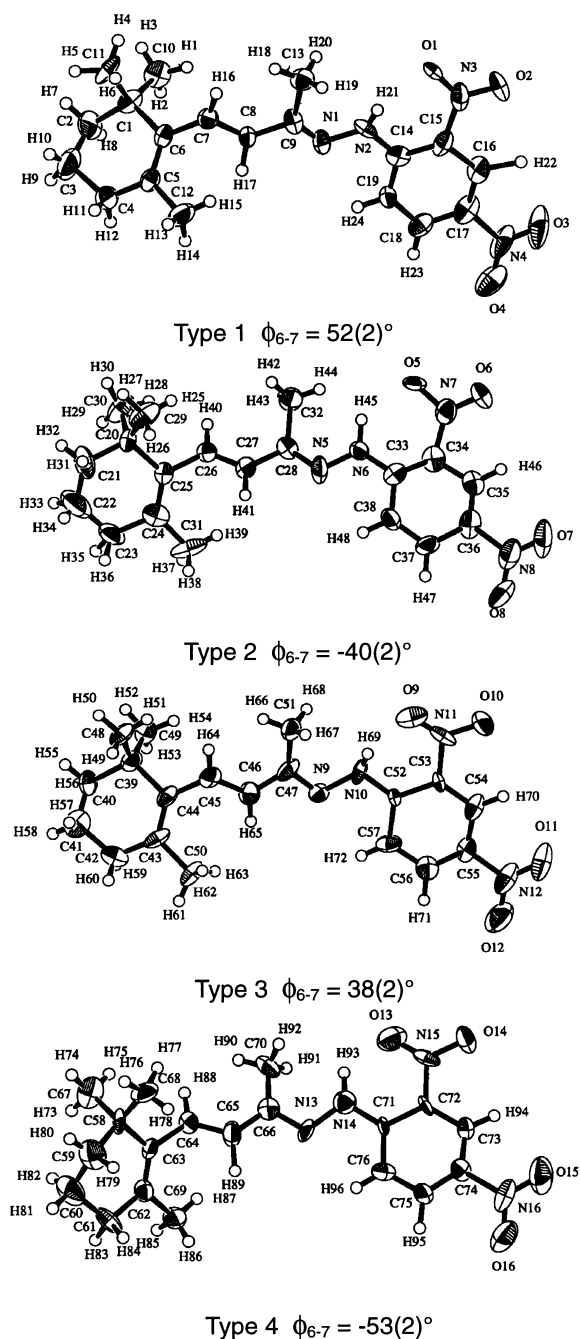

Type 1 $\phi_{6-7} = 52(2)°$

Type 2 $\phi_{6-7} = -40(2)°$

Type 3 $\phi_{6-7} = 38(2)°$

Type 4 $\phi_{6-7} = -53(2)°$

Fig. 2 ORTEP view of the four asymmetric molecules of β-IDNPH in the crystal.

Theoretical calculations

The structures of β-IDNPH were determined at cryogenic temperature but, as already mentioned, the molecular structures determined by X-ray crystallography in this study are not perfectly reliable. In addition, molecular structures in solution are not necessary the same as those in the crystalline state.
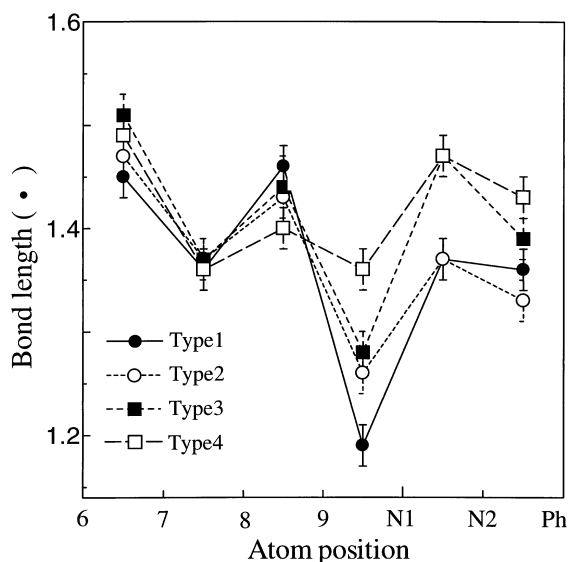
Fig. 3 Comparison of the bond lengths of the four asymmetric molecules of β-IDNPH in the crystal.

Therefore, we must take another approach to determine the precise molecular structure that is applicable for the quantitative prediction of the molecular hyperpolarizability. Here, we take a theoretical approach using both semi-empirical and non-empirical molecular orbital calculations, and perform the calculations of β-IDNPH and its component molecules, i.e. β-ionone and DNPH.

β-Ionone

The geometry was first optimized semi-empirically by means of the MNDO-AM1 method and, finally, it was optimized using *ab initio* molecular orbital calculations. Vibrational analysis was also performed. As a consequence, we found two stable structures around the C8—C9 bond of β-ionone. We called them Type I and Type II structures and they are shown in Fig. 4.

Figure 4 also compares the observed and calculated infrared (IR) spectra of β-ionone. The observed spectral shape is well reproduced by taking the Type I and II structures into account. The 1697 and 1676 cm^{-1} lines were assigned to the C=O stretching modes of the Type I and II structures, respectively.

DNPH

The same type of calculation was performed for DNPH, and the results reproduced well the observed IR spectra by taking account of the combination of various conformers around the N—N and C—M bonds. We also performed calculations of the optical absorption spectra of DNPH using a ZINDO-CI method. DNPH gave rise to two absorption bands around 340 and 410 nm as shown in Fig. 5. The former band was assigned to a HOMO → LUMO + 1 transition, while the latter band to HOMO → LUMO (HOMO, highest occupied molecular orbital; LUMO, lowest unoccupied molecular orbital). As illustrated in Fig. 5, HOMO showed an electron distribution localized around the hydrazine part, while LUMO and LUMO + 1 showed an electron distribution localized around the *ortho-* and *para*-sites of the NO_2 orbital, respectively.

β-IDNPH

β-IDNPH gave rise to two absorption bands around 390 and 640 nm as shown in Fig. 6. By inference from the results of DNPH, the origins of these two bands were assigned, respectively, to HOMO → LUMO + 1 and HOMO → LUMO transitions. We could successfully reproduce the IR spectral pattern of β-IDNPH by performing calculations on an appropriate model. However, a detailed description is not described here because of space limitations.
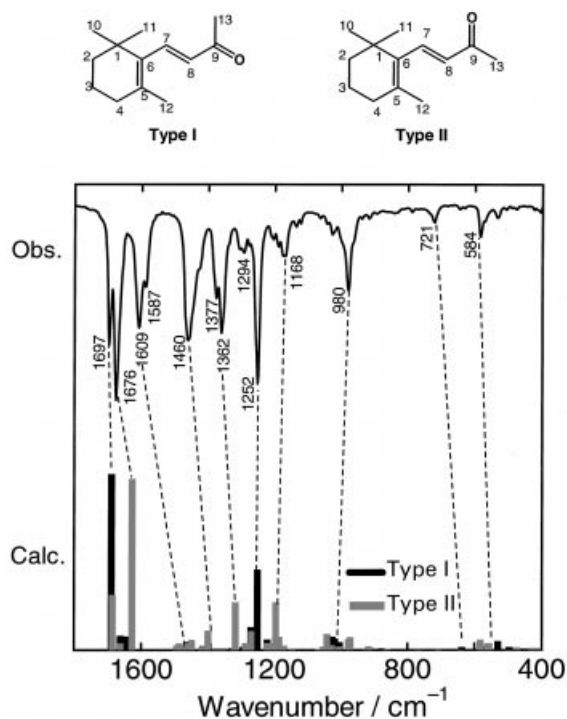
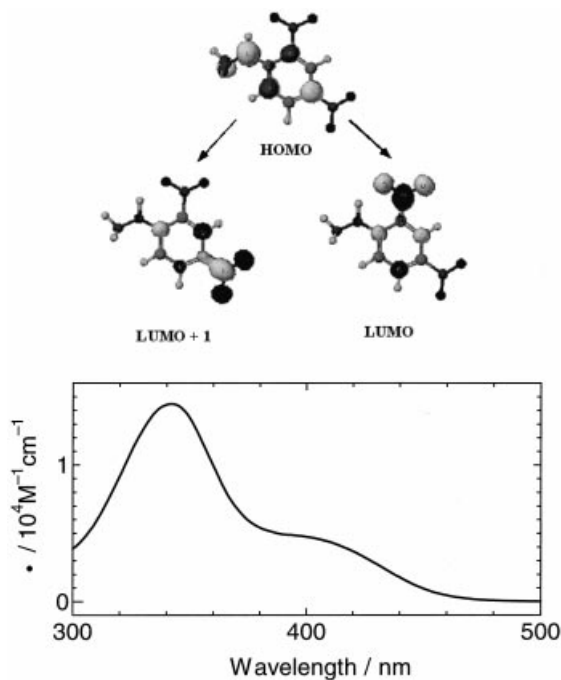**Fig. 4** Observed and calculated IR spectra of β-ionone.

Fig. 5 Optical absorption spectrum of DNPH in benzene and the assignment of transitions based on ZINDO-CI molecular orbital calculations.

STARK SPECTROSCOPY OF POLAR CAROTENOID ANALOGUES

Third-order non-linear optical materials have attracted much attention owing to their potential for photonic applications such as all-optical switching and optical computing. Recently, Marder *et al*. [14] reported that compounds in which an electron-accepting group was introduced into the polyene backbone
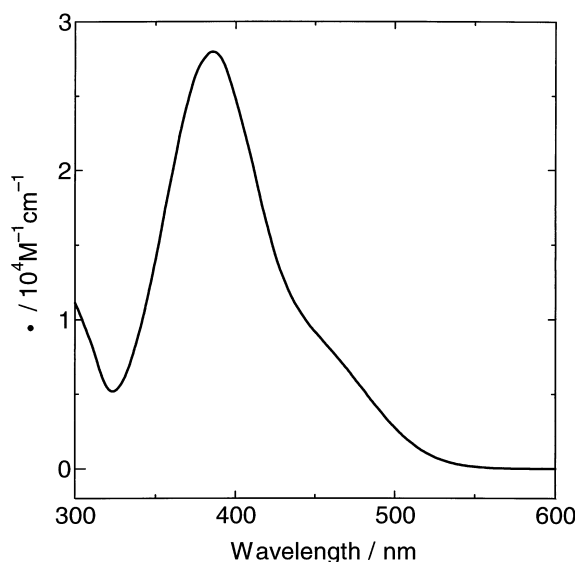
Fig. 6 Optical absorption spectrum of β-IDNPH in benzene.

of carotenoids, namely polar carotenoid analogues, show the largest third-order non-linearity among organic compounds ever studied. We have also tried to develop a novel class of third-order non-linear materials using carotenoid as a structural motif; we report the molecular and crystal structures of 2-(all-*trans*-retinylidene)-indan-1,3-dione [15].

Principles of Stark spectroscopy

Based on perturbation theory applied to a two-level model, the linear and non-linear polarizabilities of molecules can be simply expressed by Eqn (3) [16].

$$\alpha_{XX} = 2\frac{M_{ge}^2}{E_{ge}}, \quad \beta_{XXX} = 6\frac{M_{ge}^2\Delta\mu}{E_{ge}^2}, \quad \gamma_{XXXX} \approx 24\frac{M_{ge}^2}{E_{ge}^3}(\Delta\mu_{ge}^2 - M_{ge}^2) \tag{3}$$

Here, E_{ge} is the transition energy between the ground and excited states, M_{ge} is the transition moment, and $\Delta\mu$ is the difference in the permanent dipole moments between the ground and excited states. As E_{ge} and M_{ge} can be determined using optical absorption spectroscopy, if the $\Delta\mu$ value can be determined, then we can calculate the non-linear polarizabilities. For this purpose, we applied Stark spectroscopy.

The application of an intense external electric field induces the slight deviation of the optical absorption spectrum of a molecule. This phenomenon is known as the Stark effect. The modulation spectrum shows a quadratic dependence on the applied electric field and can be expressed as Eqn (4) [17].

$$\Delta A(\nu, F, \chi) = F_{int}^2 \left[A_\chi A(\nu) + \frac{B_\chi}{15h} \frac{\nu\, d(A(\nu)/\nu)}{d\nu} + \frac{C_\chi}{30h^2} \frac{\nu\, d^2(A(\nu)/\nu)}{d\nu^2} \right] \tag{4a}$$

$$A_\chi = \frac{1}{30(kT)^2}[3(\hat{p}\cdot\mu_g)^2 - \mu_g^2](3\cos^2\chi - 1) \tag{4b}$$

$$B_\chi = \frac{5}{kT}(\Delta\mu\cdot\mu_g) + \frac{1}{kT}[3(\hat{p}\cdot\Delta\mu)(\hat{p}\cdot\mu_g) - \Delta\mu\cdot\mu_g](3\cos^2\chi - 1) \tag{4c}$$

$$C_\chi = 5\Delta\mu^2 + [3(\hat{p}\cdot\Delta\mu)^2 - \Delta\mu^2](3\cos^2\chi - 1) \tag{4d}$$

Therefore, the modulation spectrum can be well accounted for by the summation of the original absorption spectrum and its first and second derivative waveforms. The coefficients A_χ, B_χ and C_χ have relevance with regard to various molecular parameters and shown an angular dependence between the

polarization of light and the applied electric field (Eqns 4b, 4c, 4d). However, in the special case of the magic angle configuration ($\chi = 54.7°$), the terms having an angular dependence disappear and the relation becomes very simple. In particular, C_χ at the magic angle directly provides us with the $\Delta\mu$ value.

Experimental set-up for Stark spectroscopy

Figure 7 shows a schematic illustration of an experimental set-up for Stark spectroscopy. We applied an external ac electric field with a frequency f to the sample, and the absorbance change induced by the field was detected at $2f$ frequency using a dual-phase lock-in amplifier.
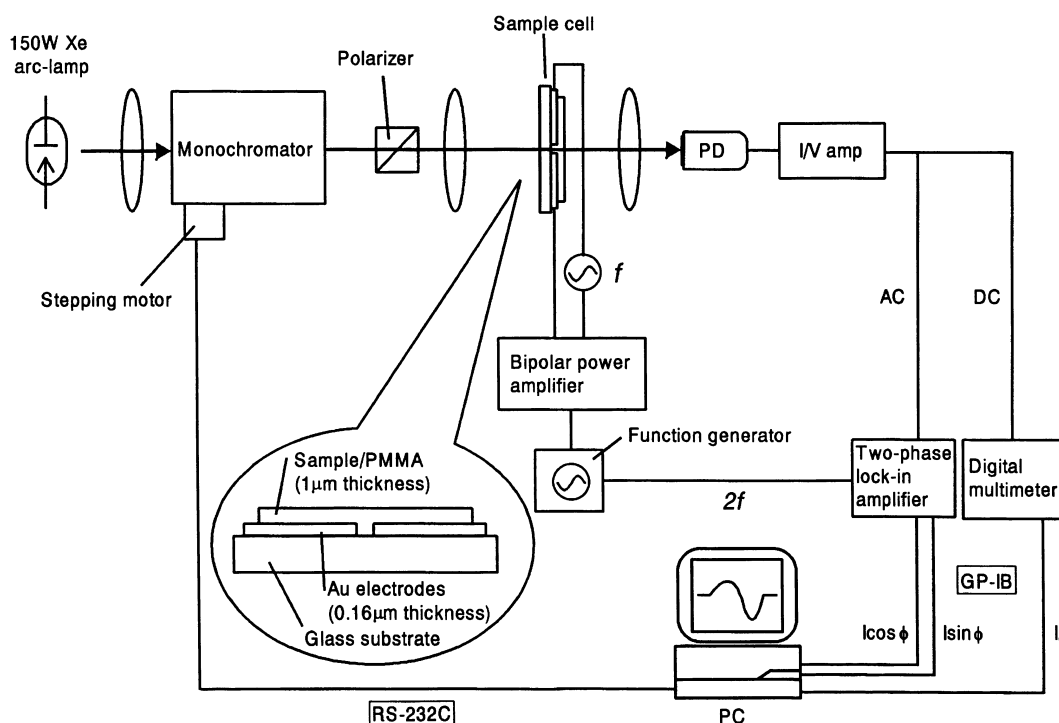

Fig. 7 Schematic description of the set up for stark spectroscopy.

The inset of Fig. 7 shows the structure of the sample cell. Gold electrodes with a gap of $50\,\mu m$ were deposited onto a glass substrate, and the sample molecules that were dispersed in a polymer (poly(methylmethacrylate), PMMA) were spin-coated on top of the electrodes. By applying $300\,V$ between these electrodes in the configuration, the sample film is exposed to an intense electric field as high as $60\,kV/cm$.

Linear and non-linear polarizabilities of polar carotenoid analogues

Figure 8 shows the chemical structures of the sample molecules studied using the present set-up of Stark spectroscopy. They are retinal (C20ald), retinylideneindane-1,3-dione (C20Ind), and its monodicyano-methylene (C20MDCInd) and bisdicyanomethylene (C20BDCInd) derivatives.

As an example of Stark spectroscopy, Fig. 9 shows the results of C20Ind. They are: (a) the absorption spectrum; its first (b) and second (c) derivative waveforms; and (d) the Stark spectrum. Circles show the observed results and the full line shows the result of spectral simulation. As shown in Fig. 9(d), we can successfully fit the observed Stark spectrum.

Table 3 summarizes the linear and non-linear polarizabilities so far determined in this investigation. The introduction of the electron-accepting indan group successfully increases the non-linear polarizabilities compared to that of the original aldehyde. Moreover, the introduction of cyano groups further
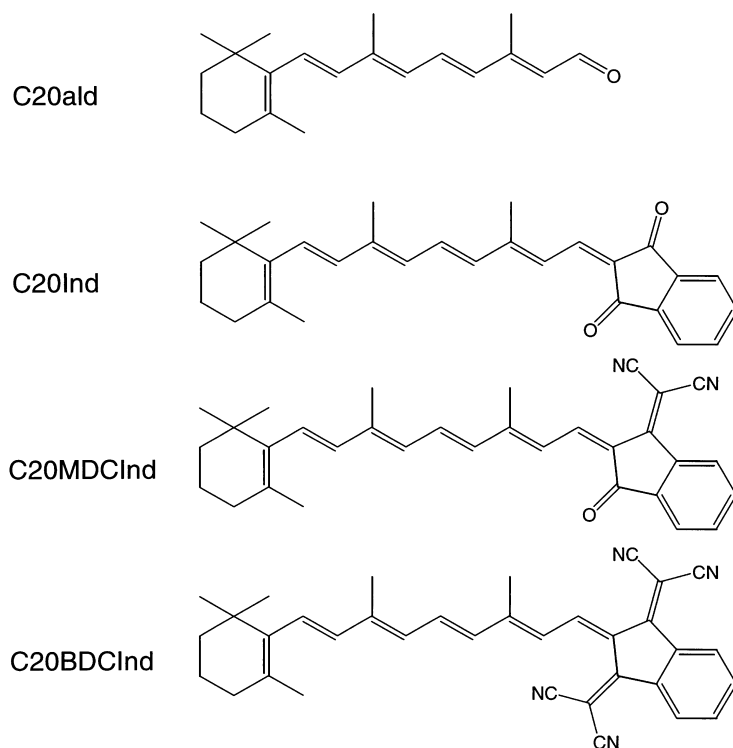
Fig. 8 Chemical structures of polar carotenoid analogues examined by Stark spectroscopy.

Table 3 Linear and non-linear polarizabilities of polar carotenoid analogues determined in this study

Compound	$|M_{gel}|$ (D)	$|\Delta\mu|$ (D)	α (10^{-23} esu)	β (10^{-28} esu)	γ (10^{-32} esu)
C20ald	8.2	10.9 ± 0.2	2.5	1.9 ± 0.03	0.04 ± 0.03
C20Ind	10.9	12.7 ± 0.2	5.8	5.2 ± 0.1	1.8 ± 0.01
C20MDCInd	10.6	12.6 ± 0.2	6.3	6.7 ± 0.1	2.9 ± 0.2
C20BDCInd	6.9	12.7 ± 0.2	2.9	6.3 ± 0.1	5.5 ± 0.2

increases the non-linear polarizabilities. It is interesting to note that the monodicyanomethyleneindan derivative (C20MDCInd) gave rise to the largest β value and hence shows the largest second-order non-linearity. On the other hand, the bisdicyanomethyleneindan derivative (C20BDCInd) gave rise to the largest γ value and hence shows the largest third-order non-linearity.

CONCLUSION

In conclusion, the structures and some optical properties of a novel polar carotenoid analogue β-IDNPH, for application as a non-linear optical material, were studied. Stark spectroscopy for the determination of non-linear polarizabilities was demonstrated. Finally, the authors hope that we will be able to communicate or compute using carotenoids in the 21st century.
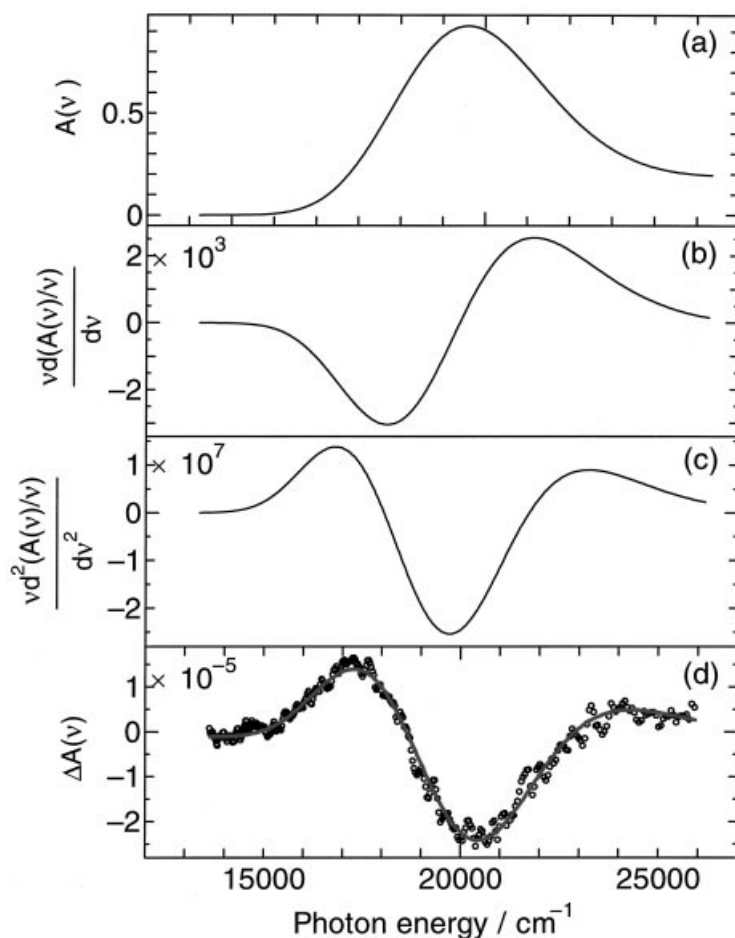
ACKNOWLEDGEMENTS

Fig. 9 (a) Optical absorption spectrum, its first (b) and second (c) derivative waveforms, and (d) Stark spectrum of C20Ind in PMMA. Circles and full line in (d) show, respectively, the experimental results and the spectral simulation using the waveforms of (b) and (c).

REFERENCES

1 D. J. Williams. *Nonlinear Optical Properties of Organic and Polymeric Materials*. ACS Symposium Series 233, American Chemical Society (1985).

2 D. S. Chemla, J. Zyss. *Nonlinear Optical Properties of Organic Molecules and Crystals*. Academic Press, Orlando (1987).

3 R. A. Hann, D. Bloor. *Organic Materials for Non-linear Optics II*. The Royal Society of Chemistry, Cambridge (1991).

4 J. Zyss. *Molecular Nonlinear Optics*. Academic Press, Boston (1994).

5 T. Kobayashi. *Nonlinear Optics of Organics and Semiconductors*. Springer, Berlin (1989).

6 H. Takahashi, S. Aoshima, Y. Tsuchiya. *IEEE Trans. Instrumentation and Measurement* **44**, 965 (1995).

7 X.-C. Zhang, X. F. Ma, Y. Jin, T.-M. Lu, E. P. Boden, P. D. Phelps, K. R. Stewart, C. P. Yakymyshyn. *Appl. Phys. Lett.* **61**, 3080 (1992).

8 H. Hashimoto, Y. Okada, H. Fujimura, M. Morioka, O. Sugihara, N. Okamoto, R. Matsushima. *Jpn. J. Appl. Phys.* **36**, 6754 (1997).

9 H. Hashimoto, Y. Okada, N. Okamoto, R. Matsushima. *J. Luminescence* (2000) in press.

10 H. Takahashi, M. Hosoda, H. Hashimoto. *Proc. 6th International Workshop on Femtosecond Technology*, pp. 191 (1999).

11   H. Takahashi, M. Hosoda, S. Aoshima, T. Yamada, H. Hashimoto. *Proc. 1999 IEEE 7th International Conference on Terahertz Electronics*, 129 (1999).

12   F. Pan, C. Bosshard, M. S. Wong, C. Serbutoviez, K. Scenk, V. Gramlich, P. Günter. *Chem. Mater.* **9**, 1328 (1997).

13   S. Folonier, Ch. Bosshard, U. Meier, G. Knöpfle, C. Serbutoviez, F. Pan, P. Günter. *J. Opt. Soc. Am.* **B3**, 593 (1997).

14   S. R. Marder, W. E. Torruellas, M. Blanchard-Desce, V. Ricci, G. I. Stegman, S. Gilmore, J. L. Brédas, J. L. Greg, U. Bublitz, S. G. Boxer. *Science* **276**, 1233 (1997).

15   H. Hashimoto, K. Hattori, Y. Okada, T. Yoda, R. Matsushima. *Jpn. J. Appl. Phys.* **37**, 4609 (1998).

16   F. Meyers, S. R. Marder, B. M. Pierce, J. L. Brédas. *J. Am. Chem. Soc.* **116**, 10703 (1994).

17   R. Mathies, L. Stryer. *Proc. Natl. Acad. Sci. USA* **73**, 2169 (1976).